



# Subsurface characterization by active and passive source geophysical methods after the 06 February 2023 earthquakes in Turkey

Hakan Karslı<sup>1</sup> · Ali Erden Babacan<sup>1</sup> · Özgenç Akın<sup>1</sup>

Received: 6 October 2023 / Accepted: 5 January 2024 / Published online: 6 February 2024  
© The Author(s) 2024

## Abstract

Two large earthquakes ( $M_w=7.7$  and  $M_w=7.6$ ) that occurred in Turkey on February 6, 2023, affected a very extent region and caused a lot of loss of life and property. This paper presents preliminary results from geophysical measurements (Seismic Refraction Tomography-SRT, Multi-Channel Surface Wave Analysis-MASW and Microtremor-MT) on eight profiles in four provinces (Kahramanmaraş, Hatay, Malatya, Gaziantep) to understand the relationship between subsurface properties and the destruction that occurs immediately after earthquakes. By analyzing the geophysical data, the dynamic-elastic properties of ground and the soil classification according to  $V_s30$  were determined. It is generally understood that the near-surface ( $< \sim 10\text{--}15$  m) units in the measurement areas are very loose, and the deeper ones ( $\geq \sim 15\text{--}20$  m) have a very porous/fractured structure. Soil classes were defined as ZD (Malatya-1, Hatay-1 and Kahramanmaraş-1) and ZC (Malatya-2, Hatay-2, Gaziantep-1,2 and Kahramanmaraş-2). In addition, by evaluating the information of strong ground motion station closest to the measurement profiles, it is observed that the PGA values versus epicenter distances are higher at stations in the zone parallel to the direction of both faults than those in the perpendicular zones. This leads directivity effect in the propagation of earthquake waves. The results indicate that one of the basic reasons for the damages is that the earthquake-ground-structure relationship has not been fully and accurately reflected in building designs. Therefore, future researches involving more geophysical data and PGA values will provide more information about the structural, physical and geotechnical properties of subsurface and definitive results.

**Keywords** Kahramanmaraş earthquakes · SRT · MASW · HVSR · PGA

---

✉ Hakan Karslı  
hkarsli@ktu.edu.tr

Ali Erden Babacan  
a.babacan@ktu.edu.tr

Özgenç Akın  
ozgencakin@ktu.edu.tr

<sup>1</sup> Department of Geophysical Engineering, Karadeniz Technical University, 61080 Trabzon, Turkey

## 1 Introduction

On February 6, 2023, two major earthquakes occurred in Turkey. As reported by the Ministry of Interior Disaster and Emergency Management Presidency (AFAD 2023), the first one was recorded at 4.17 am (01.17 GMT) in Kahramanmaraş-Pazarcık (epicenter coordinates:  $37.288^{\circ}$  N– $37.043^{\circ}$  E,  $M_w=7.7$ ,  $H=8.6$  km) on the NE-SW trending Eastern Anatolian Fault Zone (EAFZ), and the second one was recorded at 13.24 pm (10.24 GMT) in Kahramanmaraş-Ekinözü (epicenter coordinates:  $38.089^{\circ}$  N– $37.239^{\circ}$  E,  $M_w=7.6$ ,  $H=7.0$  km) on the D-W trending Çardak Fault (ÇF). These earthquakes occurred with a time difference of about 9 h and affected 11 provinces in a wide area of about 400 km from their epicenters. More than a hundred thousand buildings have been destroyed or severely and moderately damaged, and more than 50,000 people have lost their lives. In the studies prepared immediately after the earthquakes, it was stated that the total length of rupture for the first earthquake (Kahramanmaraş-Pazarcık earthquake) reached ~350 km, and the second earthquake (Kahramanmaraş-Ekinözü) reached ~160 km (Melgar et al. 2023; Goldberg et al. 2023). However, according to the strong ground motion records of the two events, field observations and information received from the people of the region, it was reported that the first earthquake was more active in Kahramanmaraş and Hatay, and the second earthquake was more active especially in Malatya (AFAD 2023). In the same report, the peak ground acceleration (PGA) of the first earthquake was recorded as  $2039 \text{ cm/s}^2$  (2.039 g) at Kahramanmaraş-Pazarcık station 4614, and the PGA of the second earthquake was recorded as  $635 \text{ cm/s}^2$  (0.635 g) at Kahramanmaraş-Göksun station no. 4612. In addition, in formal institutional reports prepared by AFAD (2023), Boğaziçi University, Kandilli Observatory and Earthquake Research Institute (KOERI 2023), Middle East Technical University (METU 2023) based on post-earthquake field observations, the main reasons why the earthquake was felt severely in such a wide area are summarized as follows: inadequate earthquake-resistant construction, lack of engineering projects in many buildings, wrong location choices for urbanization, and finally inadequate, incomplete and faulty earthquake-ground-structure relationship including the physical properties and behaviors of the earth. Moreover, several investigations reported that the main reason for the damage observed in the buildings was the inconsistency between the earthquake code requirements and the design/construction practices of the damaged buildings (Ozkula et al. 2023; Işık 2023). Especially, Ozkula et al. (2023) also specified that the concrete strength of the damaged buildings was quite low (i.e., 6–10 MPa).

Before starting any engineering construction, it is very important to evaluate the suitability of the site for the type of construction to be carried out. In this context, knowledge of the depth profiles and physical properties of the earth is necessary to understand the causes of damage after earthquakes as well as before earthquakes. Because, the most important causes of destruction and damage in earthquakes are the deformations that occur during the propagation of earthquake waves through any subsurface. Therefore, the damage that occurs anywhere after earthquakes due to the behavior of the ground increases the importance of knowing the soil properties in a sensitive manner. After many devastating earthquakes, geoscientific studies to investigate the causes of the damages have shown that the amplitudes of the earthquake waves and the dominant periods increase especially in weakly resistant soils and that liquefaction occurs in sandy soils where the groundwater level is shallower than 20 m. Moreover, it has been observed that earthquakes cause resonance between soil and structure, causing significant structural damage and loss of life even at distances of more than 100 km from the earthquake location (Tezcan and İpek

1973; Tezcan et al. 1978; Cassaro and Romero 1987; Kaptan and Tezcan 2012; Akkaya et al. 2015; Keçeli and Cevher 2015; Cevher and Keçeli 2018). The best examples of them are Russia-Alma Ata in 1964, Turkey-Gediz in 1970, Romania-Vrancea in 1977, Mexico City in 1985, Istanbul Gölçük in 1999, Van in 2011, Elazığ-Sivrice in 2019 and Aegean Sea-Sisam Island in 2020. In addition, it has been determined that the concave and convex structure of the underground bedrock topography causes earthquake waves to focus on the center of the basin and the edges of the basin, respectively, while sand lenses and dykes cause the earthquake waves to be channeled and therefore increase the amplitude of the waves (Keçeli 2012).

In the investigation of the physical properties and mechanical behavior of the ground, fast and noninvasive geophysical measurements have been commonly used in recent years, as opposed to traditional (drilling and open-pit) methods which are generally invasive, noneconomic and time consuming. Parameters obtained by conventional methods are static, whereas geophysical parameters are dynamic. Therefore, geophysical methods are considered the most reliable methods for seismic site characterization (Azwin et al. 2013; Sitharam et al. 2018) and are indispensable tools for seismologists and civil engineers to obtain sufficient information about subsurface structure and lithology (Benson and Yuhr 2002).

The depth profile of the subsurface allows the layered structure of the ground and the bedrock topography to be imaged. Besides, the physical properties and behavior of the ground include the determination of parameters such as Poisson's ratio, and modulus of shear, elasticity (Young's) and incompressibility (bulk) and the period of the soil vibration dominant, the soil amplification, the soil liquefaction and the available bearing capacity of geological units. Therefore, damages from earthquakes are directly related not only to structural characteristics but also to local geology and dynamic behavior of the soil. The seismic soil response at a given location is greatly influenced by the local geology and soil properties (Moustafa et al. 2007; Martínez-Pagán et al. 2018; Molina et al. 2018). This highlights the importance of site classification in areas of high seismicity or seismic vulnerability.

Shallow seismic refraction (SSR) and multichannel analysis of surface waves (MASWs) techniques are widely used to evaluate the basic design parameters of buildings and to explain soil and rock-related problems. Seismic refraction tomography (SRT) which is an inverse solution techniques of first arrival times from SSR data, and MASW techniques are time and cost effective in obtaining longitudinal wave (P-wave) and shear wave (S-wave) velocities of the subsurface materials, respectively. The SRT technique allows to obtain the 2D and 3D velocity structure of the subsurface (Rucker 2000; Leucci et al. 2006; Raghu Kanth and Iyengar 2007; Babacan et al. 2018), faults (Buddensick et al. 2008; Khalil and Hanafy 2016) and soil/rock parameters (Azwin et al. 2013; Keçeli 2012; Maraió et al. 2014; Sheehan et al. 2005; Vanlı Senkaya et al. 2020) without damaging the natural subsurface state. However, SRT technique is widely used in determining the interfaces between layers with different seismic velocities, engineering purposes, environmental projects, geo-technical investigations, dam safety and groundwater studies (Bridle 2006; Yılmaz et al. 2006; Hodgkinson and Brown 2005).

MASW is an active source method that is generally used to estimate the variation of S-wave velocity with depth at shallow depths (30 m), and its average for 30 m depth is called  $V_{s30}$ . It also helps to determine the engineering and elastic parameters of the soil. However, while the application of the MASW technique in the field is less time consuming, the processing of the recorded data requires high precision (Park et al. 1999). S-wave velocity ( $V_s$ ) is calculated by inverse solution of the Rayleigh wave

dispersion curve (phase velocity versus frequency) from the MASW data. Practically, the subsurface velocity-thickness model that gives the best fit between the measured and calculated dispersion curves is tried to be obtained (Xia et al. 1998, 1999; Miller et al. 1999).

Therefore, SRT and MASW techniques are used to estimate the physical properties of the soil materials and the engineering parameters required for the design of the structures to be built on it (Keçeli 2012; Kanli 2009; Yılmaz et al. 2009; Uhlemann et al. 2016). P- and S-wave velocities ( $V_p$  and  $V_s$ ) are recognized to provide useful information for assessing liquefaction potential, natural vibration frequencies and the performance of ground motion (Bauer et al. 2001; Hunter et al. 1993; Tinsley and Fumal 1985). Hence, significant information about the stiffness of the soil is the key parameter for understanding the ground shaking response of soils and is highly effective for predicting soil amplification (Borcherdt 1994).

In recent years, Single Station Microtremor (MT) measurements have been utilized to determine local soil conditions. This method, developed by Nakamura (1989) and commonly referred to as horizontal (H)/vertical (V) spectral ratio (HVSr), is widely used as a fast, easy and highly reliable method for determining the dominant period and soil amplification characteristics (Lermo and Chavez-Garcia 1994). In the method, environmental noises (with frequency  $f < \sim 1.0$  Hz) are recorded as three components at a single station. A series of data processing operations such as detrending, filtering, windowing and smoothing are applied to the recorded data to obtain the HVSr curve, which is calculated as the ratio of the mean of the squares of the horizontal components to the vertical component. The frequency value ( $f_0$ ) corresponding to the maximum amplitude of the HVSr curve is determined as the soil dominant frequency (or period =  $1/f_0$ ) value (Lachet and Bard 1994; Bard 1998). In addition, HVSr value is also used to determine the thickness of the soil layers on the bedrock by means of experimental relationships (Field and Jacop 1993; Birgören et al. 1998; Özalaybey et al. 2011). After Nakamura (1989), the method has been widely used by many researchers in engineering applications to analyses local soil conditions (Gallipoli and Mucciarelli 2009; Akkaya 2015; Akin and Sayıl 2016; Pamuk et al. 2017a-b; Öztürk et al. 2021).

The aim of this study is to obtain a preliminary knowledge about the relationship between the damages and physical properties of subsurface in four provinces including Kahramanmaraş, Hatay, Gaziantep, and Malatya after devastating earthquakes. Geophysical data were acquired by authors on date from February 19 to 23, 2023, in the suitable locations in those provinces. In this context, SRT, MASW and MT measurements were made at eight different locations and two in each province, and then by analyzing the all data, physical, dynamic-elastic and geotechnical parameters of the locations were obtained. In addition, site classification based on  $V_s30$  value was done according to TEBC code which is adapted from NEHRP. Furthermore, the information (epicenter distance, maximum peak ground acceleration-PGA,  $V_s30$ ) for the strong ground motion station closest to the measurement profiles was evaluated and discussed in terms of damages and the subsurface characteristics obtained in this study. It should be noted that the data presented and conclusions drawn by the authors are the preliminary findings. Therefore, future researches involving more geophysical data and considering more PGA values will provide more comprehensive information about the structure, physical and geotechnical properties of subsurface.

## 2 Regional geology and seismotectonic

The locations of both earthquake and seismicity of the study area are shown in Fig. 1. Immediately after the main shocks, a large number of aftershocks are observed within a 15-day period, and this aftershock activity clearly increased the background seismicity of the region much more than before the main shocks. The region covering four provinces (Fig. 1), where geophysical measurements are carried out and where earthquakes are most effective, is within the influence area of the EAFZ, one of the most effective and active fault systems in Turkey, and is also very active in terms of current tectonics. EAFZ is approximately 580 km long (Duman and Emre 2013), NE-trending left-lateral strike-slip

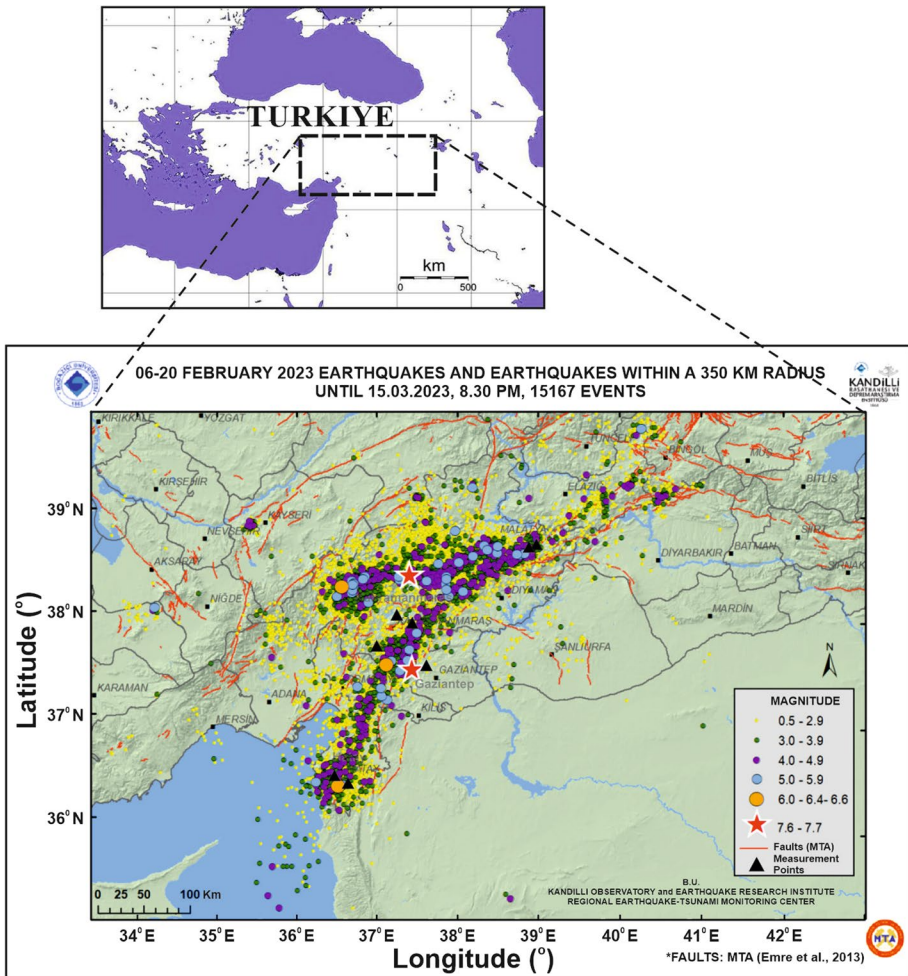


**Fig. 1** Faults, earthquake locations, affected provinces and epicenter distributions of earthquakes ( $M \geq 4.0$ ) that occurred between February 6, 2023, and February 20, 2023 (modified from AFAD (2023)). Red stars and black triangles indicate the epicenter locations of the two earthquakes that occurred on February 6, 2023, and measurements locations in this study, respectively

fault system consisting of many fault segments varying 50 km to 145 km (Duman and Emre 2013; Şahin and Öksüm 2021) that lies and between Karlıova triple junction point in Bingöl and Hatay Provinces (AFAD 2023; METU 2023). The EAFZ forms a major boundary between the Anatolian and Arabian Plates (Reilinger et al. 2006; Moreno et al. 2011), and the Arabian plate is moving toward the north-east with respect to the Anatolian plate at approximately  $11 \pm 2$  mm/year according to GPS data (Çetin et al. 2003; AFAD 2023). Historically, many large earthquakes have occurred along the EAFZ (some of them are Antakya, 1822,  $M_s=7.5$ ; Karlıova, 1866,  $M_s=7.2$ ; Amik Lake, 1872,  $M_s=7.2$ ; Hazar, 1875,  $M_s=7.1$ ; Malatya, 1893,  $M_s=7.1$ ). = 7.1) occurred and caused loss of life and property (Kartal and Kadiroğlu 2013; Öztürk 2020). However, during the instrumental period, the devastating 1971 Bingöl ( $M_s=6.5$ ), 1975 Diyarbakır-Lice ( $M_w=6.6$ ) and 2020 Elazığ-Sivrice ( $M_w=6.5$ ) earthquakes occurred.

As reported in AFAD (2020), the region commonly contains Precambrian-Paleozoic and Mesozoic aged South-east Anatolian autochthonous or Arabian Platform sediments. On the platform sediments consisting of schist, gneiss, marble, limestone, sandstone, quartzite and shale rock units, there are complex units including allochthones ophiolite units, volcanic units and deep-sea sediments settled in the post-Upper Cretaceous region. The geomorphology of the region is shaped by the movements of faults, and it is seen that quaternary aged wide and thick alluvial materials (sand, clay, gravel and their alternations) with weak strength character, reaching up to 300 m, are stratified between the high mountains. However, sedimentary rocks dominate as the bedrock and the groundwater level is quite shallow (Palutoğlu and Şaşmaz 2017).

### 3 Methods and data analysis

Within the scope of this study, well-known and widely preferred geophysical methods were used to determine the geometric structure, physical properties and dynamic behaviors of the earth. To evaluate the basic parameters for engineering structures and to explain the problems related to subsurface materials (rock + soil), data were acquired with SRT, MASW and MT methods, which are applied quickly and economically and evaluated in line with the principles of the methods. The SSR method includes the analysis of seismograms recorded in receivers placed in an order on the earth's surface, during the propagation of seismic energy sent into the ground from an artificial source, of directly incident waves and critically refracted waves at the interfaces of lithological units with different velocities. The first arrival times read from these seismograms are evaluated with the delay time (minus-plus and/or generalized reciprocal time method-GRM) and SRT techniques, and the seismic velocities of the lithological layers forming the ground structure (P-wave velocity,  $V_p$  and S-wave velocity,  $V_s$ ), thickness and 2D velocity model are obtained. The SRT technique has a strong ability to characterize lateral and vertical velocity gradients in the study area. Moreover, it is ideal in environments with extreme topography or complex structures near the surface and where the operator has little or no prior knowledge of the subsurface structure (Zhu and McMechan 1989). Therefore, in any site characterization, the interpretation of SSR data with the SRT technique is highly effective compared to delay time techniques (Redpath 1973; Azwin et al. 2013). Therefore, SRT sections are widely used in determining the interfaces between layers, calculating the dynamic-elastic parameters of the ground, engineering and environmental projects, geotechnical research,



determining the locations of covered faults, surveying dam sites and investigating the groundwater aquifer (Bridle 2006; Yılmaz et al. 2006; Lankston 1989).

The most important cause of damage occurring during an earthquake is the dynamic behavior of the ground during the passage of shear and surface waves. Shear stress, the basic parameter that determines the behavior of the ground under dynamic loads, is calculated from the shear wave velocity ( $V_s$ ); therefore, this velocity value is extremely vital in the static project design of the structure. The most commonly and safely used method for determining  $V_s$  is MASW (Xia et al 1999; Park et al. 1999). In this method, the near-surface shear wave velocity structure is obtained as a function of depth (1D- $V_s$ ) by inverting the dispersion curve (change of phase velocity against frequency) of surface waves (Rayleigh and Love) recorded using an active source. Three basic steps of the method include data acquisition, data processing and inversion. Rayleigh type surface waves are analyzed when vertical component receivers are used in data acquisition. However, for Love type surface waves, horizontal component receivers are used. According to the 1D- $V_s$  change, geotechnical characterization of the place, including the density-stiffness evaluation, soil-rock distinction and soil class, is performed. In particular, the  $V_{s30}$  value is the key parameter used all over the world and taken into account in soil classification tables (NEHRP 2003; CEN 2005; TEBC 2018).

It is based on the principle of recording environmental vibrations (amplitudes varying between 0.1 and 1.0 microns and periods varying between 0.05 and 2 s) for a certain period of time (mostly > 30 min) in three components (East–West, North–South and Vertical). Since the single station MT method offers practical application opportunities, it has found widespread application in earthquake engineering applications and microzonation studies in recent years. The method is also known as the Nakamura (1989) HVSR method and is used to determine the ground dominant vibration period and ground amplification characteristics. In particular, it is used to obtain the resonance frequency, which is an important cause of collapse in earthquakes, and to estimate the bedrock depth using empirical formulas between frequency and thickness (Birgören et al. 2009; Zor et al. 2010; Özalaybey et al. 2011; Tun et al. 2016; Molnar et al. 2018; Buyuksarac et al. 2021).

### 3.1 Data acquisition

In this study, SSR, MASW and MT (approximately at the midpoint of the profiles) data were acquired in eight profiles, two different profiles in each of the four provinces where the earthquake caused heavy damage. Six of the profiles were determined in places that exemplify the subsurface structure where there are buildings that were completely demolished or partly destroyed and damaged to different degrees. In these areas, since the streets and avenues are asphalt and concrete paved surfaces, geophones are placed on the ground with holder boxes. During data acquisition, especially, MT measurements were negatively affected by noise from working machinery, human mobility and traffic due to wreck removal activities in the surrounding area. One of the other two profiles is located at the place where the large landslide (splitting/opening) occurred in the olive grove in Tepehan Village of Hatay Province Altınözü District after the Pazarcık earthquake, and the other is on the surface trace of the fault line in Tevekkeli Village of Kahramanmaraş Dulkadiroğlu Municipality. Some images from the data acquisition locations are presented in Fig. 2.

A 24-channel PASI 16S24-U model seismograph and a 4.5 Hz vertical component geophone, a 10 kg hammer and hardened plastic (chestamite) table with 20 cm diameter and 5 cm thick were used to acquire the SR and MASW data. MT data were recorded



**Fig. 2** Images from measurement locations: (a-1,2) Malayta-Yeşilyurt, (b-1,2) Hatay-Defne and Teppehan, (c-1,2) Gaziantep-İbrahimli and Nurdağı and (d-1,2) Kahramanmaraş-Tevekkeli and City Center. The slip of EAF in this place was observed as 4 m

for 30–45 min with a three component CMG 6-TD Güralp seismometer. Images of the equipment and connections used in seismic and microtremor data acquisition at the time of measurement are shown in Fig. 3.

The field source-receiver layouts of SR and MASW data are given in Fig. 4, and the data acquisition parameters of all measurements are given in Tables 1 and 2. To gather the MASW data, the end-on ( $S_1$ ) and end-off ( $S_7$ ) shots in the SR profile were done, and only the recording time and sampling time were updated.

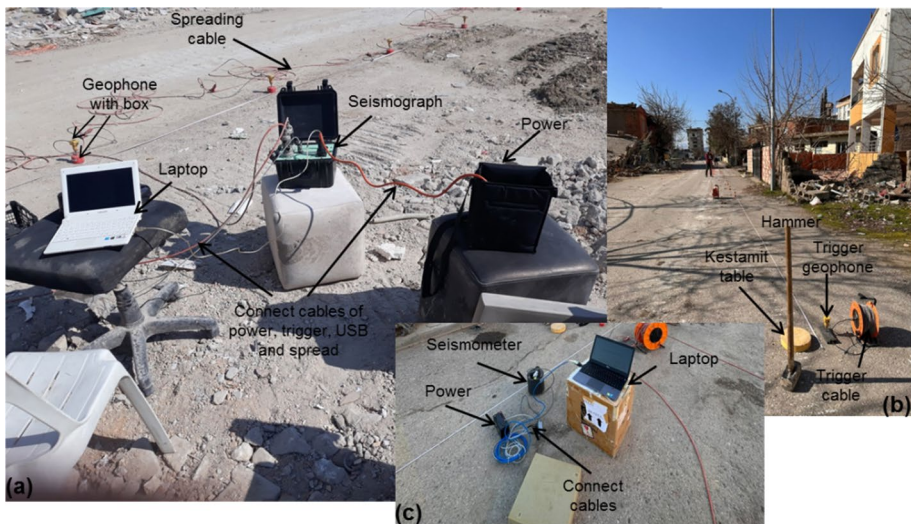


**Fig. 3** Images of the measurement equipment during the field operation: a and b SR and MASW and c MT equipment and connection cables



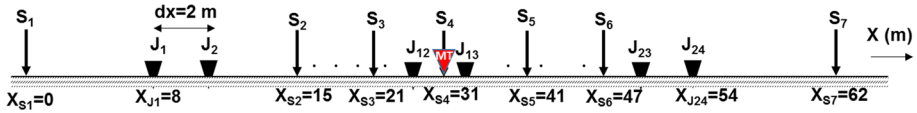


**Fig. 4** The layout of the source-receivers for SR and MASW data acquisition:  $S_{1,2,\dots}$ ,  $X_{S1,2,\dots}$  and  $X_{J1,2,\dots}$  show source points, source and geophone distance.  $dx$  and  $MT$  show geophone interval and location of the MT measurement, respectively

**Table 1** The data recorder parameters for SR, MASW and MT measurements

Method	Record time, $T$ (s)	Sampling time, $dt$ (ms)	Shots in Fig. 4, $S_k$ ( $k = 1, 2, \dots, 7$ ) and MT points	Vertical stack, $N$
SR	1.0	0.25	All	3
MASW	2.0	1.0	$S_1$ and $S_7$	3
MT	1800	10	$S_4$	

### 3.2 Data processing

All data obtained from each measurement method were evaluated according to the theoretical principles of the methods used. The 2D P-wave velocity model and geometry (layered structure, discontinuities and bedrock depth) of the subsurface were obtained from tomographic inversion of the first arrival times peaked from SSR data and will be referred to as seismic refraction tomography (SRT). One-dimensional shear wave velocity (1D- $V_s$ )-depth profile was obtained from MASW data, and  $V_{s30}$  value was calculated for soil classification. By applying a series of data processing to the three component MT data at each measurement point, the soil dominant vibration frequency (or period) and H/V ratio (HVSr) of the study area were determined. Analysis of SSR and MASW data was carried out with SeisImager/SW (2022), and analysis of MT data was implemented by Geopsy (2020) software.

An evaluation summary of SSR data is shown in Fig. 5 for an example data (Gaziantep-Nurdađı data) recorded within the scope of this study. First arrival times (direct and refracted waves) from each shot data are peaked (first arrivals for all shots are shown with green and red lines on the middle shot data in Fig. 5a) and plotted against receiver distances (blue lines in Fig. 5b). For an initial model, a 2D P-wave velocity model is obtained by iterative tomographic inversion (Fig. 5c). The solution starts with a homogeneous initial velocity model laterally; the solution is iterated until the root mean square (RMS) error between the measured time values and the calculated time values (black lines in Fig. 5b) is minimized. In our inversion analysis, generally, the RMS errors were below 5% within the 10 iterations. While the velocity-depth model (Fig. 5c) obtained when the minimum error is reached is interpreted physically according to lateral and vertical velocity changes, if there is drilling information about the profile, geophysical information can be interpreted geologically. However, since there is no drilling information in this profile, the interpretation was physically made only. Accordingly, the 2B- $V_p$  section in Fig. 5c is interpreted as three layers including loose soils at first layer ( $Z = \sim 0\text{--}5$  m, 300–1000 m/s), changing from medium tight to very tight at the second layer ( $Z = \sim 5\text{--}17$  m, 1000–1800 m/s) and changing from soft to hard rock at the third layer ( $Z > 17$  m,  $V_p > 1800$  m/s). However, a

**Table 2** Soil classification according to  $V_{s30}$  value in TEBC (2018)

Site class	Rock and soil description	Average for 30 m deep		
		$(V_s)_{30}$ (m/s)	$(N60)_{30}$ (blow/30 cm)	$(CU)_{30}$ (kPa)
ZA	Hard rock	> 1500	–	–
ZB	Less weathered or medium hard rock	760–1500	–	–
ZC	Very stiff soils or very fractured weak rocks	360–760	> 50	> 250
ZD	Medium stiff or stiff soils	180–360	15–50	70–250
ZE	Soil or any profile with more than 3 m of soft clay is defined as soil with $PI > 20$ , $w \geq 40\%$ and $C_u < 25$ kPa	< 180	< 15	< 70
ZF	Soils with the risk of collapse and potential collapse under the influence of earthquakes (liquefiable soils, highly sensitive clays, collapsible weak cemented soils, etc.) Clays with a total thickness of more than 3 m of peat and/or high organic content High plasticity ( $PI > 50$ ) clays with a total thickness of more than 8 m Very thick ( $> 35$ m) soft or medium stiff clays			

$PI$  Plasticity Index,  $w$  water content,  $C_u$  Undrained shear strength

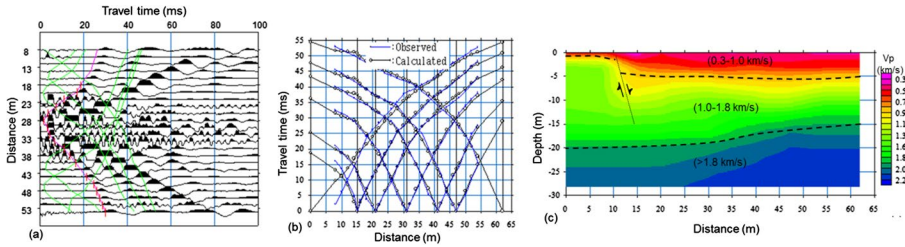


**Fig. 5** The evaluation of the Gaziantep-Nurdağı (Gaziantep-2 in Table 4) SSR data: **a** picking on first arrival times on shot data, **b** the graph of the measured and calculated first arrival times and **c** 2D- $V_p$  section obtained by SRT inversion and its interpretation

covered normal fault anomaly was detected in the  $X=5\text{--}20$  m distance range of the section. In addition, it is seen that the bedrock depth decreases from  $Z= \sim 20$  m at  $X=0$  m to  $Z= \sim 15$  m at  $X=62$  m, that is, it becomes shallower.

The evaluation steps of MASW data are shown in Fig. 6 for the measurement profile in the Central Tevekkeli village of Kahramanmaraş Province. The steps include firstly the acquisition of the data from the field (Fig. 6a), imaging through frequency–phase velocity ( $f\text{--}c$ ) transformation (Fig. 6b) and secondly peaking the fundamental mode dispersion curve (phase velocity values versus frequency) in the widest frequency range (Fig. 6c). Finally, Fig. 6d indicates the 1D- $V_s$  depth profile by inverting this dispersion curve. The phase shift technique (Park et al. 1998) was used for the  $f\text{--}c$  transformation of the time record in Fig. 6a, and the damped least squares algorithm was used for the inversion process, with 20 iterations. Thus, by taking advantage of the change of the 1B- $V_s$  depth profile up to a depth of 30 m, the  $V_{s30}$  value, which is a very important and necessary parameter in the calculation of the dynamic-elastic and engineering parameters of the ground, geotechnical designs and earthquake hazard assessment studies, was calculated with the following formula.

$$V_s = \frac{30}{\sum_{i=1}^N \frac{h_i}{V_{si}}}$$

where,  $h_i$  and  $V_{si}$  present, respectively, thickness and shear wave velocity of the  $i$ th layer for 30 m depth, and  $N$  is the number of layers.

By analyzing the MT data, the steps of determining the soil dominant vibration frequency  $f_0$  (or  $T_0 = 1/f_0$ ) and H/V ratio are presented in Fig. 7 for three component (Vertical-V, North–South-NS and East–West-EW) data with 30 min recorded in Malatya-2 location. The data were processed with the open and freely available "Geopsy" program. In data processing, trending and a band-pass filter with a cutoff frequency of 0.5–20 Hz were applied to the raw data, respectively. Then, the spectra of all three components (Fig. 7b) were calculated for 25-s windows (Fig. 7a) (each colored line represents the spectrum of one window) in accordance with the SESAME criteria. These spectra were proportioned according to Nakamura's technique, and the H/V curve was obtained (Fig. 7c). By evaluating the H/V curve together with the spectra of each component (red frame area in b), the soil dominant frequency value ( $f_0$ ) on the H/V curve was determined (vertical gray bars in c). The black thick line in Fig. 7c shows the average of the spectra from each window, and the dashed lines show the standard deviation limits.

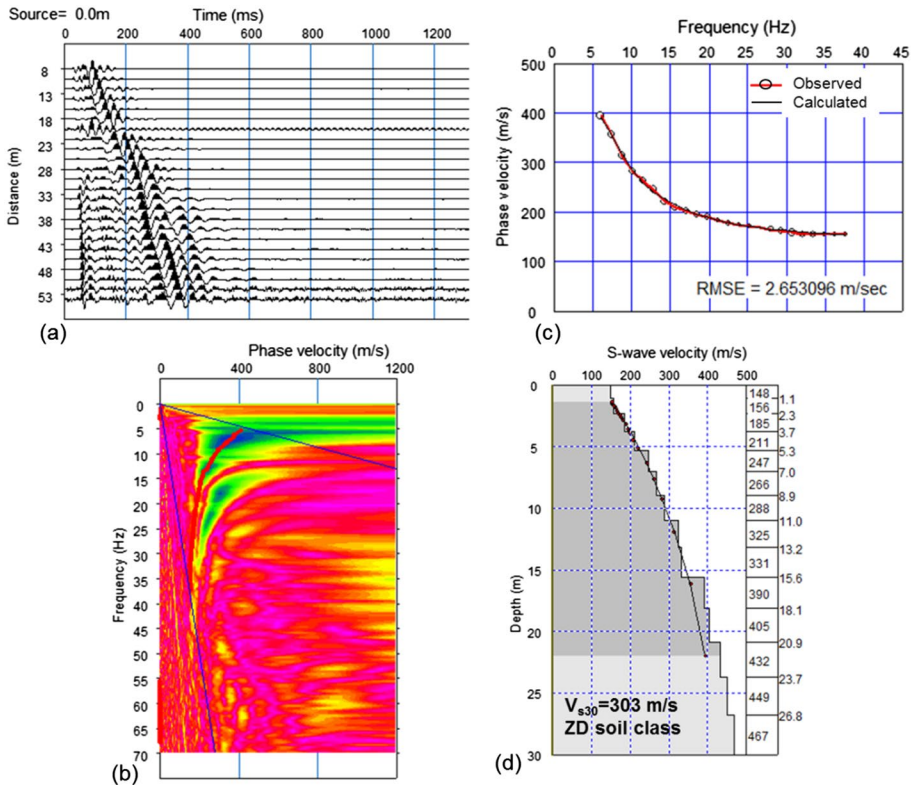


**Fig. 6** Evaluation stages of MASW data recorded in Kahramanmaraş Province Central Tevekkeli village: **a** MASW data, **b** f-c image, **c** Rayleigh wave dispersion curve and **d** 1D- $V_s$  depth profile produced from the inversion of the dispersion curve. The  $V_{s30}$  is calculated as 303 m/s, and this value represents ZD soil class according to TEBC

## 4 Results and discussions

### 4.1 Evaluation and interpretation of profiles

Since there is no previously reported borehole information for measurement locations in this study, lithological soil and rock identification could not be done. In contrast, S-wave velocity information was attributed according to TEBC (2018) and Karlı et al. (2021). SRT sections and 1D- $V_s$  depth profiles are given in Figs. 8 and 9. By correlating 2D- $V_p$  velocity sections and 1D- $V_s$  depth profiles, approximate velocity interfaces were determined, generally three layer subsurface models were created and the average P and S-wave velocities of each layer were obtained. However, using these seismic velocities, elastic (density, the modulus of Young's, Shear and Bulk) and geotechnical (soil classification in Table 2 according to  $V_{s30}$  value, available bearing capacity, soil dominant vibration periods and amplification) parameters for each layer were calculated according to the formulas given in Table 3 and listed in Table 4. The soil dominant vibration periods were also calculated based on the  $V_{s30}$  value empirically for comparison with those obtained from MT data.

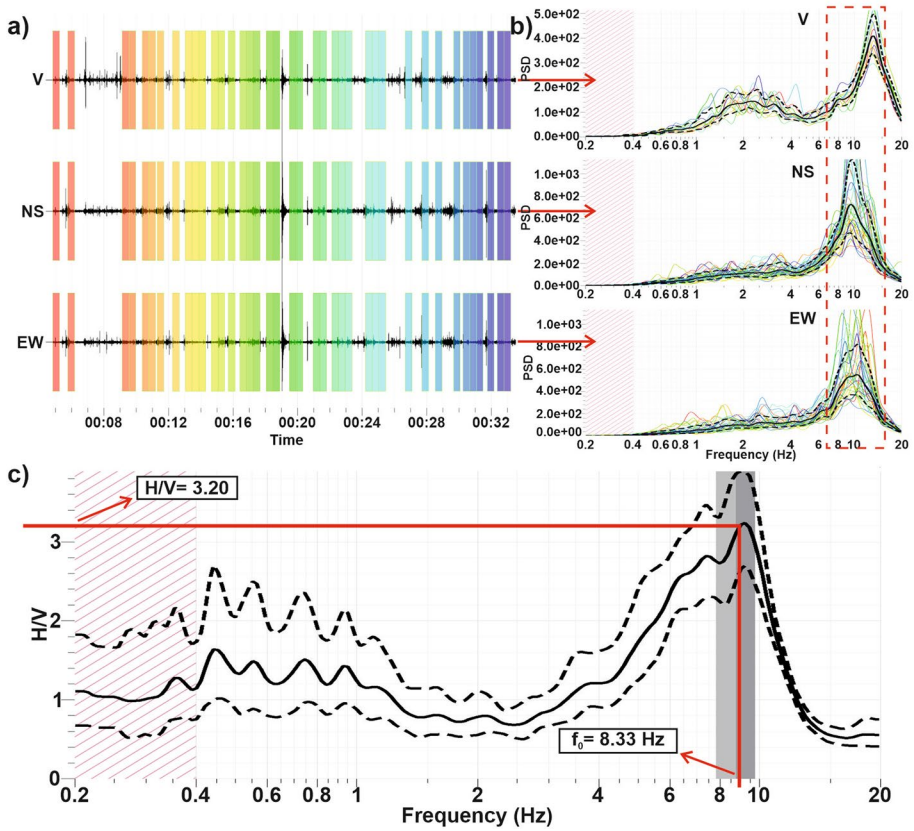


**Fig. 7** The analyzing of the MT data: **a** windowed of the three component MT data, **b** spectra for each component and **c** H/VSR curve. In **c**, solid and dashed lines indicate H/VSR curve and standard deviations, respectively. PSD in (b) means power spectral density

Even though they are located quite far from each other, SRT sections clearly present similar subsurface velocity models. In general, loose and less stiff soil units from the surface to a depth of ~7 m ( $V_p=0.3\text{--}1.0$  km/s,  $V_s=0.16\text{--}0.3$  km/s) and below that ~7–18 m thick ( $V_p=1.0\text{--}1.8$  km/s,  $V_s=0.3\text{--}0.6$  km/s) medium stiff-stiffer soil units are common. In the deeper part, the geological units with high weathering levels or soft rocks with  $V_p > 1.8$  km/s,  $V_s > 0.6$  km/s are placed. According to  $V_s/30$  values, the soils in the study areas are classified as ZD (Malatya-1, Hatay-1 and KMaras-1) meaning the moderate stiff and ZC (Malatya-2, Hatay-2, Gaziantep-1, 2 and KMaras-2) meaning fractured weak rock.

The ratio of P- and S-wave velocities,  $V_p/V_s$ , is a key parameter that provides information about the physical properties, lithological changes, mineral compositions, clay contents, grain sizes, fracture densities, porosity, fluid saturations and types of soil and rocks (Tatham 1982; Salem 2000; Uyanik 2011), and recently, it has been widely used for the characterization of soil and rocks (Keçeli 2012). According to Telford et al. (1976), Poisson’s ratio is calculated based on the  $V_p/V_s$  ratio, and these two parameters are linearly related. Therefore, while the Poisson ratio approaches zero for very hard and solid rocks, it approaches 0.5 for very loose soils, highly weathered sediments and fluids (friable



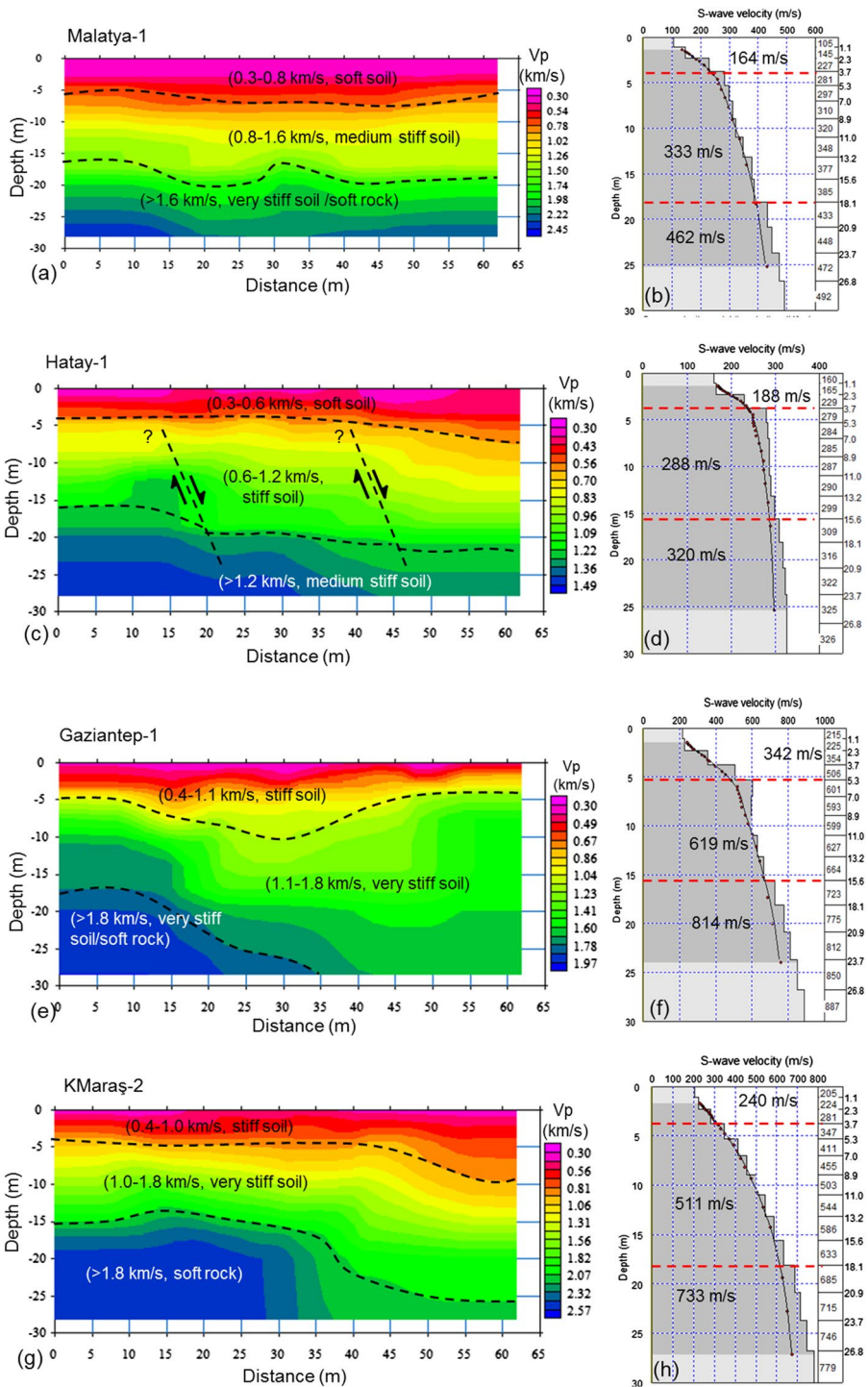


**Fig. 8** 2D- $V_p$  velocity sections and 1D- $V_s$  depth profiles: **a, b** Malatya-1, **c, d** Hatay-1, **e, f** Gaziantep-1 and **g, h** Kahramanmaraş-2. The dotted black curve in **b, d, f, and h** indicates Rayleigh wave phase velocity variation

sediments or fluids). For moderate stiff materials, it is generally around  $\sim 0.25$ . The  $V_p/V_s$  and Poisson values vary between 2.19–4.43 and 0.37–0.47, respectively. However, weak materials and high porosity rocks have high Poisson's ratio and vice-versa. Accordingly, for the subsurface models obtained in all profiles, the first layer corresponds to weakly resistant, the second layer to moderately resistant and the third layer to resistant but possibly porous rock units.

The densities of lithological units were calculated with the empirical formula proposed by Uyanık and Çatlıoğlu (2015, 2019), which allows the combined use of P- and S-wave velocities and better represents low-velocity subsurface units. Thus, density values vary between 1.72 and 2.20  $\text{gr}/\text{cm}^3$ , indicating low-density subsurface units in the  $\sim 0$ –18 m depth range and partially dense sedimentary rocks at deeper depths.

In order to understand the level of resistance (endurance) of the geological units in the study areas against earthquake dynamic forces, thanks to seismic velocities, the elastic modulus including the shear (a measure of the solidity of the material), elasticity (or Young's, a measure of the hardness and strength of the material) and bulk (or incompressibility, a measure of compression under forces) modules is calculated and presented in Table 4.

When the obtained values are evaluated according to Bowles (1996), the geological units can be defined in three groups as: (1) loose ( $\mu \leq 600 \text{ kg}/\text{cm}^2$ ,  $E \leq 2000 \text{ kg}/\text{cm}^2$ ), (2) moderately stiff and medium solid ( $600 < \mu \leq 3000 \text{ kg}/\text{cm}^2$ ,  $2000 < E \leq 10,000 \text{ kg}/\text{cm}^2$ ) and (3) strong to stronger ( $\mu > 3000 \text{ kg}/\text{cm}^2$ ,  $E > 10,000 \text{ kg}/\text{cm}^2$ ). However, according to ASTM (1978), the incompressibility levels of these units can be defined as low ( $400 < K \leq 10,000 \text{ kg}/\text{cm}^2$ ), medium ( $10,000 < K \leq 40,000 \text{ kg}/\text{cm}^2$ ) and high ( $40,000 < K \leq 100,000 \text{ kg}/\text{cm}^2$ ).

Allowable bearing capacity,  $Q_a$ , is the load that the ground can carry without being exposed to any excessive deformation (collapse, settlement, sprain, shear fracture, shear, etc.) (Tezcan et al. 2009; Keçeli 2012; Uyanık and Gördesli 2013). The allowable bearing capacity values calculated for this study are lower than  $10 \text{ kg}/\text{cm}^2$  ( $\sim 1 \text{ MPa}$ ). Values of  $Q_a$  less than  $4.0 \text{ kg}/\text{cm}^2$  generally correspond to layers containing slightly to moderately compacted near-surface geological units, while values of  $Q_a$  between 4.0 and  $8.0 \text{ kg}/\text{cm}^2$  represent layers containing more compacted soil units and mostly highly weathered rocks.

Soil amplification values calculated according to Midorikawa (1987) vary between 1.5 and 2.30. On the other hand, the ground dominant periods ( $T_0$  and  $MT_0$ ) calculated from  $V_s30$  and directly determined by MT (HVSR) are generally consistent, except for Malatya-1 and 2 profiles, and vary between 0.12 and 0.40 s. When evaluated according to Ansal et al. (2001, 2004), these values indicate that the soil amplification and soil dominant vibration periods in the study areas are at low-medium levels. Moreover, for the soil dominant vibration period values according to Kanai and Tanaka (1961), it is defined as “rock-stiff sandy gravel units” and/or “alluvium consisting of sandy-gravelly stiff clay” and is in harmony with soil classifications based on velocities obtained from seismic profiles. In addition, the periods suggest that especially collapsed/seriously damaged 4–5 floor buildings are under the effect of resonance.

## 4.2 Possible relations between ground properties and damage observations

The findings of the present study provide more important clues that the damage levels that occurred after the earthquake and were directly observed in the field by the authors of this

**Fig. 9** 2D- $V_p$  velocity sections and 1D- $V_s$  depth profiles: **a, b** Malatya-2, **c, d** Hatay-2, **e, f** Gaziantep-2 and **g, h** Kahramanmaraş-1. The dotted black curve in **b, d, f,** and **h** indicates Rayleigh wave phase velocity variation. In **g,** considering the direction perpendicular to the plane of the screen or paper, the cross sign ( $\otimes$ ) and the dotted circle ( $\odot$ ) indicate a block moving away and a block approaching, respectively

paper may be related to subsurface characteristics and behavior. Observations and relationships are summarized in Table 5.

Table 6 presents some information about strong ground motion (acceleration) stations located close to the measurement profiles. Information about the stations was obtained from AFAD. The selected stations are the closest stations that have both acceleration records for both earthquakes ( $M_w=7.7$  and  $M_w=7.6$ ) that occurred on February 6, 2023, and  $V_{s30}$  values determined for the installation of the stations. Although the distances between measurement profiles and stations are less than 30 km, except for Malatya-1 and 2 profiles, other stations are very close to our measurement profiles. According to the epicenter distances in Table 6, the closest station to the epicenter locations of both the first and second earthquakes is station no. 4625 ( $R_1=28.40$  km and  $R_2=65.22$  km), while the farthest station is station no. 3136 ( $R_1=148.38$  km and  $R_2=231.36$  km). When the  $V_{s30}$  values obtained previously for the installation of earthquake recording stations and the  $V_{s30}$  values determined in this study are compared, except for the  $V_{s30}$  value of station no. 4406 ( $V_{s30}=815$  m/s), all the other values are in compliance with the  $V_{s30}$  values obtained in this study, and inherently, it is seen that they are in the same soil class. The two closest measurement profiles (Malatya-1 and 2) to station no. 4406 are at a distance of  $\sim 28.0$  km, and normally, the geological units within this distance may differ. Therefore, the  $V_{s30}$  value ( $V_{s30}=815$  m/s) at this station shows ZC soil class which means less weathered or moderate hard rock according to Table 2. However, the distance between Gaziantep-1 measurement profile location and station no. 2703 is  $\sim 3.5$  km, and while the  $V_{s30}$  value of the station is 758 m/s, the  $V_{s30}$  value obtained in this study is 578 m/s. Normally, both values represent ZC soil class (360–760 m/s) as defined in Table 2. However, the value of  $V_{s30}=758$  m/s is very close to the upper limit of the ZC soil class and therefore indicates a stiffer soil or less weathered rock than the measurement profile location ( $V_{s30}=578$  m/s). Thus, this difference of  $\sim 180$  m/s between both  $V_{s30}$  values can be considered as a result of variability in local soil properties (degree of weathering, compactness, porosity, subsurface topography, etc.) at very close distances.

Figure 10a shows the distribution of maximum PGA values listed in Table 6 for the first and second earthquakes. The difference between the magnitudes of earthquakes is as  $\Delta M_w=0.1$ . The energies of both events are calculated by using the formula,  $\log E=5.24+1.44M_w$  (URL-1 <https://www.usgs.gov/programs/earthquake-hazards/earthquake-magnitude-energy-release-and-shaking-intensity> (Accessed on November 17, 2023),  $M_w$ : moment magnitude). When the energies of both earthquakes are proportioned ( $E_2$  for  $M_w=7.7$  and  $E_1$  for  $M_w=7.6$ ), it is seen that  $E_2/E_1 \cong 1.40$ . According to this difference, although the energy of the first earthquake was approximately 1.40 by times more than the second earthquake, it can be said that they produced similar amounts of energy. In this context, in the epicenter distance-PGA distribution in Fig. 10a, the accelerations of the first earthquake were less than  $\text{PGA}=250$   $\text{cm/s}^2$  at stations no. 4406 and 2703, but larger at other stations, and it was quite high  $\text{PGA}=638.32$   $\text{cm/s}^2$  at station no. 3124 which is 140.11 km away. On the other hand, the highest acceleration value of the second earthquake was observed at station no.4406 ( $467.20$   $\text{cm/s}^2$ ), while it was less than  $100$   $\text{cm/s}^2$  at other stations. However, while acceleration values in general tend to decrease significantly with distance, it is seen that the acceleration

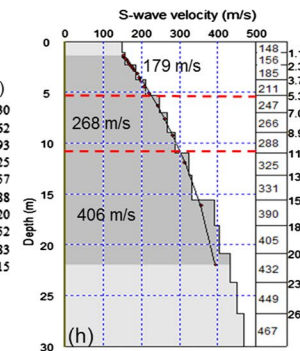
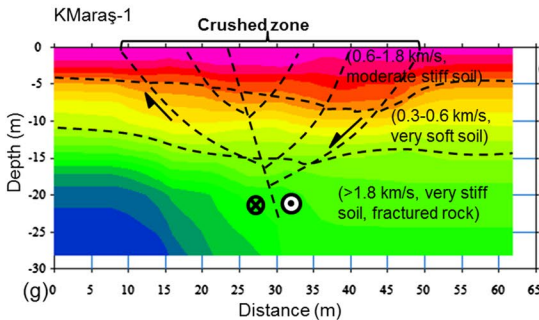
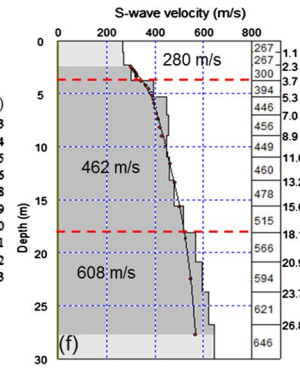
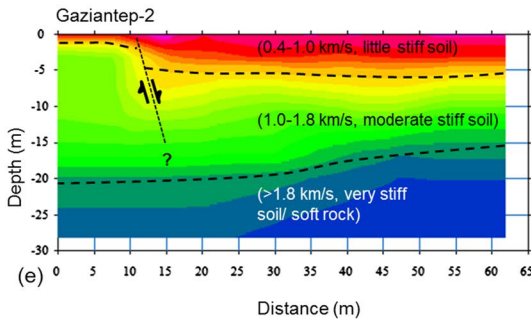
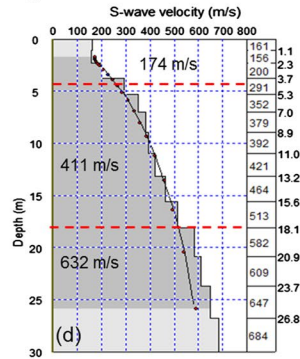
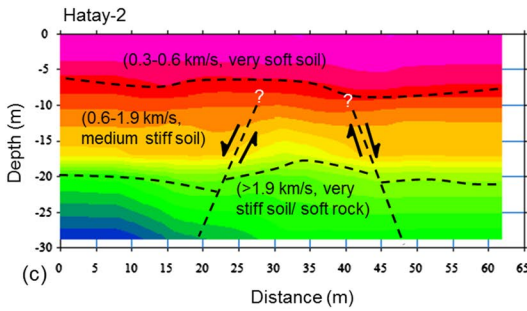
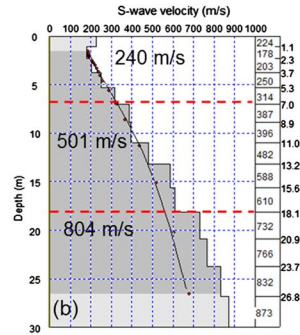
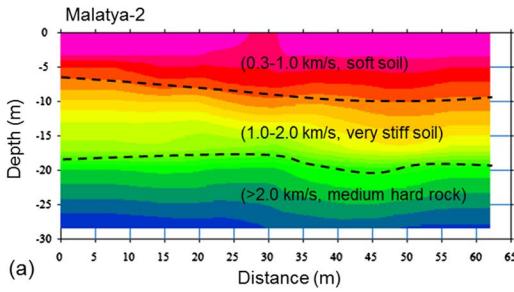


**Table 3** Definition of elastic and geotechnical parameters used in this study

Parameter	Equation	References
Density ( $\rho$ )	$\rho = 0.7 (V_p V_s)^{0.08}$	Uyanık and Çathoğlu (2015), Uyanık (2019)
Poisson ratio ( $\sigma$ )	$\sigma = \frac{0.5V_p^2 - V_s^2}{(V_p^2 - V_s^2)}$	Telford et al. (1976), Geldart and Sheriff (2004)
Elastisite or Young's modulus ( $E$ )	$E = 2\rho V_s^2(1 + \sigma)$	
Shear or rigidity modulus ( $\mu$ )	$\mu = \rho V_s^2$ or $\mu = \frac{E}{2(1+\sigma)}$	
Bulk modulus ( $K$ )	$K = E/3(1-2\sigma)$	
Allowable bearing capacity ( $q_a$ )	$Qa = \rho * V_s / F$ ( $F$ : safety factor is used as $V_p/V_s$ ratio in this study)	Tezcan et al. (2009)
Soil dominant vibration period ( $T_0$ )	$T_0 = 4 * H / V_{S30}$	Keçeli (2012)
Soil amplification ( $A$ )	$A = 68 * V_{S30}^{-0.6}$	Midorikawa (1987)

values at stations 3124 and 3136 increased abnormally for the first earthquake. Nevertheless, it is understood that the epicenter distance-PGA change of the stations listed in Table 6 does not show a linear behavior. For example, station no. 3124 is 140.11 km away from the first earthquake location,  $PGA = 638.32 \text{ cm/s}^2$ , and 226.42 km away from the second earthquake location,  $PGA = 32.18 \text{ cm/s}^2$ . Similarly, station 3136 is 148.38 km away from the first earthquake and 236.36 km away from the second earthquake, and the peak acceleration values are  $PGA = 534.22 \text{ cm/s}^2$  and  $PGA = 22.79 \text{ cm/s}^2$ , respectively. Although there is a distance of ~88 km between the epicenter distances of both earthquakes for station no. 3136, the dramatic decrease in PGA values of the second earthquake at the same stations is quite striking. Another interesting observation in Fig. 10a is that, although they are approximately at the same distance, the PGA values at stations 2703–8002–4625 and 4625–4406 are quite different from each other. It is clear that these differences cannot be explained only by epicenter distances and shallow subsurface characteristics of the station locations.

Considering the locations of the acceleration recording stations in Fig. 10b and the directions of the faults (or rupture direction) where the earthquakes occurred, it can be said that the direction of the fault and the PGA values are related. Namely, while station no. 2703 is in the zone approximately perpendicular to the direction of movement of NF+PF and EAF (first earthquake), stations no. 8002 and 4625 are located in the zone almost in the direction of the rupture direction. Similarly, while station 4425 is in the zone perpendicular to SF+ÇF (second earthquake), station 4406 is seen to be located in the same zone which is approximately parallel to the direction of these faults. Thus, these observations support that the magnitude of the accelerations and therefore the damages caused by earthquakes may be related not only to subsurface properties but also to the directivity effect in the propagation of earthquake waves (especially destructive surface waves).



**Table 4** Elastic and geotechnical parameters at the profiles

Profile loca- tion	Center coordinate of profiles (degree)	E		N		Layer No	Vp (m/s)	Vs (m/s)	Vp/Vs	$\rho$ (gr/ cm <sup>3</sup> )	$\sigma$	$\mu$ (kg/ cm <sup>2</sup> )	E (kg/ cm <sup>2</sup> )	K (kg/ cm <sup>2</sup> )	Qa (kg/ cm <sup>2</sup> )	Vs30 (m/s)	A	T0= 4H/ Vs30 (s)	MT0 (s)	Soil class
		38.352209	38.352271	36.231807	36.160881															
Malatya-1 (Yeşilyurt)	38.300577	38.352209	1	550	164	3.35	1.74	0.45	468	1358	4640	0.85	320	2.14	0.38	0.12	ZD			
			2	1200	333	3.60	1.96	0.46	2173	6339	25326	1.81								
			3	1600	462	3.46	2.06	0.45	4397	12791	46873	2.75								
Malatya-2 (Yeşilyurt)	38.294293	38.352271	1	650	240	2.71	1.82	0.42	1048	2979	6292	1.61	440	1.76	0.27	0.12	ZC			
			2	1500	501	2.99	2.07	0.44	5196	14935	39647	3.46								
Hatay-1 (Defne)	36.165484	36.231807	1	450	188	2.39	1.73	0.39	611	1705	2688	1.36	282	2.30	0.43	0.37	ZD			
			2	900	288	3.13	1.90	0.44	1576	4548	13289	1.75								
			3	1200	320	3.75	1.96	0.46	2007	5867	25548	1.67								
Hatay-2 (Tepehan)	36.221200	36.160881	1	450	174	2.59	1.72	0.41	521	1471	2789	1.16	393	1.89	0.31	0.31	ZC			
			2	1250	411	3.04	2.00	0.44	3378	9726	26745	2.70								
			3	1900	632	3.01	2.15	0.44	8588	24694	66165	4.52								
Gantep-1 (Ibrahimli)	37.338549	37.073868	1	750	342	2.19	1.90	0.37	2222	6084	7724	2.96	578	1.50	0.21	0.25	ZC			
			2	1450	619	2.34	2.10	0.39	8046	22346	33424	5.55								
			3	1800	814	2.21	2.18	0.37	14445	39620	51373	8.02								
Gantep-2 (Nurdagi)	36.742259	37.179804	1	700	280	2.50	1.86	0.40	1458	4097	7170	2.08	467	1.70	0.26	0.22	ZC			
			2	1450	462	3.14	2.05	0.44	4376	12632	37267	3.02								
			3	1800	608	2.96	2.13	0.44	7874	22607	58514	4.37								

**Table 4** (continued)

Profile loca- tion	Center coordinate of profiles (degree)	E		N		Layer No	Vp (m/s)	Vs (m/s)	Vp/Vs	$\rho$ (gr/ cm <sup>3</sup> )	$\sigma$	$\mu$ (kg/ cm <sup>2</sup> )	E (kg/ cm <sup>2</sup> )	K (kg/ cm <sup>2</sup> )	Qa (kg/ cm <sup>2</sup> )	Vs 30 (m/s)	A	T0= 4H/ Vs30 (s)	MT0 (s)	Soil class							
KMaraş-1 (Tevekkeli)	37.019114	37.467787	1	450	179	2.51	1.73	0.41	554	1559	2764	1.23	303	2.21	0.40	0.36	ZD										
																		2	1050	268	3.92	1.91	0.47	1372	4020	19229	1.31
																		3	1800	406	4.43	2.06	0.47	3396	10005	62217	1.89
KMaraş-2 (Merkez)	36.933970	37.569180	1	700	240	2.92	1.83	0.43	1054	3022	7562	1.51	491	1.65	0.24	0.16	ZC										
																		2	1500	511	2.94	2.07	0.43	5405	15506	39368	3.60
																		3	1800	733	2.46	2.16	0.40	11605	32509	54510	6.45

**Table 5** Damage observations and their relationship to ground properties

Profile name	Damage observations	Relation with subsurface properties
Malatya-1 (Yeşilyurt)	Although this location is ~ 200 km away from the 1st earthquake (Pazarçık earthquake) epicenter and ~ 120 km away from the second earthquake (Ekinözü) epicenter, there are several buildings completely destroyed and damaged to varying degrees as shown in Fig. 2a-1	All findings for this profile indicate a generally thick and very weak ground structure. The parameters $Vp/Vs \geq 3.35$ , $\sigma \geq 0.45$ , $Qa \leq \sim 3.0 \text{ kg/cm}^2$ for all layers clearly indicate that the water content of the soil units is high and very loose, and the rock units are quite porous or highly weathered. On the other hand, it is thought that the values of $A = 2.14$ and $T_0 = 0.38 \text{ s}$ increased the earthquake load on the soil, and therefore, the earthquake-earth motion could not be adequately reflected in the design of the collapsed buildings in this area
Malatya-2 (Yeşilyurt)	It is ~ 1 km away from Malatya-1 location. However, no destroyed buildings were observed. However, slight damage was observed on the exterior of the buildings as shown in Fig. 2a-1	In general, it is thought that there are very compact soil units up to ~ 15 m depth and engineering bedrock at a deeper level as shown in Fig. 9a. The medium can be considered as moderate solid. However, in the bedrock, $Vp/Vs = 2.49$ and $\sigma = 0.4$ indicate that the rock structure is hard but porous
Hatay-1 (Defne)	Although this location is ~ 200 km away from the first earthquake (Pazarçık) epicenter and ~ 300 km away from the second earthquake (Ekinözü) epicenter and almost all of the surrounding buildings are newly constructed, there are many destroyed and severely damaged buildings as shown in Fig. 2b-1	The findings in this profile support that the soil layer is thick and quite loose, the water content is high and the strength is very low. As seen in the SRT section (Fig. 8c), it was evaluated that there may be covered faults
Hatay-2 (Tepehan)	This location is in the south-west of the Hatay-1 location and is ~ 25 km away from it. This area is known for being frequently on the agenda in the written and visual media as a result of the large splitting and/or opening (or advanced ground failure) in the olive grove due to earthquakes. Therefore, it is aimed to exemplify the soil structure and geophysical properties in this area as shown in Fig. 2b-2	Due to the landslide in the form of opening/splitting observed in the field, the subsurface lithology could be observed visually. It was observed a stratification of claystone-marlstone units to a depth of approximately ~ 50 m. Seismic velocities indicate that these units are quite loose up to a depth of ~ 5.0 m, but become stiffer, harder and brittle (can be thought of as glass or biscuit) as they go deeper. The SRT result clearly indicates a compressing structure where has been caused by the large splitting event as shown in Fig. 9c

**Table 5** (continued)

Profile name	Damage observations	Relation with subsurface properties
Gaziantep-1 (İbrahimli)	This location is ~50 km away from the 1st earthquake (Pazarçık epicenter) and ~200 km away from the 2nd earthquake (Ekinözü) including two-blocks (twin block) on the same foundation and shopping floor was destroyed but the other was slightly damaged. In fact, no buildings damaged by the earthquake were observed in its immediate vicinity as shown in Fig. 2c-1	According to the soil class, ZC, it has a compact soil structure. When the parameters in Table 1 are examined, the highest $V_{s30}$ value, strength parameters and soil bearing capacity are obtained in this profile, whereas the lowest $V_p/V_s$ , $\sigma_v$ and $T_0$ values are for this profile. However, while thick and very stiffer units with P-wave velocities varying between 0.4–1.8 km/s are dominant up to ~18 m in the SRT section in Fig. 8d, it can be considered that a possible deeper rock unit could be fractured-cracked or porous rock. The fact that the 1D- $V_s$ depth profile in Fig. 8f shows increasing $V_s$ values toward depth supports this opinion. However, as can be clearly seen from the 2B- $V_p$ section, it is noteworthy that the soil layer gradually thickened after ~15 m from the source point. Beyond all this, the collapse of one of the twin blocks (corresponding to between 25 and 55 m, according to the SRT section) can be explained in two ways: (1) the soil thickening between 25 and 55 m was not taken into account in the static project when the building was being constructed (such as foundation design, ground improvement, etc.), (2) negative interventions may have been made to the supporting column and beam elements of the collapsed block (such as cutting columns and beams)
Gaziantep-2 (Nurdâğı)	Both high-rise and low-rise buildings have collapsed and severely damaged. On the other hand, low-rise (1–2-story houses with a garden layout) most of which collapsed were observed to be very old (columnless masonry, adobe, etc.) manufactures from the observations made from their wrecks as shown in Fig. 2c-2	According to the parameters in Table 1, the soil properties are generally similar to Gaziantep-1. Differently, the SRT results in obtained in this profile indicate the presence of a covered normal fault (Fig. 9e). However, an important reason for the damages observed around this profile may be related to the buildings' exposure to high intensity, especially from the first earthquake, and the poor quality of the materials used in the many old (masonry, masonry, etc.) structures in the surrounding area. Therefore, it is a strong possibility that the earthquake-ground-structure relationship was either not taken into account completely or accurately in the design of collapsed and damaged structures in this area

**Table 5** (continued)

Profile name	Damage observations	Relation with subsurface properties
Kahramanmaraş-1 (Tevekkeli)	This location is on an agricultural land and is the closest location to the first earthquake epicenter (Pazarçık) (~ 35 km) and ~ 65 km away from the second earthquake epicenter (Ekinözü). Most of the houses made of masonry in the village in the immediate vicinity of the location (> 2 km away) were destroyed. Geophysical measurements for observing the effect of left-lateral strike-slip fault on seismic data have been conducted and for this, the seismic profile is laid perpendicular to the fault direction. The slip of the fault was measured as 4 m as shown in Fig. 2d-1	Near surface signs of the fault are interpreted on the SRT cross section. Accordingly, it is observed a flower structure, which is a typical strike-slip fault descriptor. The decrease in seismic velocity toward the depth can also be considered as the effect of the presence of fractures in the shallow bedrock due to the fault (Fig. 9g and h). Moreover, the fault traces, which can be followed from the surface, can be followed to a depth of ~ 15 m, according to the SRT section obtained for this profile (Fig. 9g). On the other hand, according to the parameters in Table 1, weak and loose soil units are dominant in this area
Kahramanmaraş-2 (City Center)	This location is ~ 50 km away from the epicenter of both earthquakes (Pazarçık, Ekinözü earthquakes). It was taken very close to the street named as Trabzon, which is the busiest living area and where the most destruction was experienced. No adverse events were observed in the buildings on both sides of the measured street, apart from very slight damage as shown in Fig. 2d-2	In this profile, it is understood that the soil units are less stiff between ~ 0–3 m depth, stiffer between ~ 3–15 m depth and after ~ 15 m depth, there are soft rock units toward the depths. However, the fact that $V_p$ and $V_s$ values are lower than expected, especially after ~ 15 m depth, strengthens the possibility that the rock unit has a very soft and porous structure. Additionally, it is noteworthy that the depth of the rock unit becomes shallower up to ~ 30 m from the beginning of the profile



**Table 6** Comparison of some information obtained from strong motion stations close to the measurement profiles in this study.  $R_1$ ,  $PGA_1$  and  $R_2$ ,  $PGA_2$  represent the epicenter distances of the first and second earthquake on February 6, 2023, respectively, and the maximum PGA values read at each station.  $V_{s30\_I}$  and  $V_{s30\_P}$  show the average shear wave velocities at 30 m depth obtained from the acceleration recording station locations and measurement profiles within the scope of this study, respectively. Stations parameters are taken from AFAD (<https://kadas.afad.gov.tr>)

Profile name	Near station code	Station coordinate (°)	Distance between locations of profile and station, L (km)	Epicenter distance, R (km)	$V_{s30\_I}$ for station (m/s)	$V_{s30\_P}$ from this study (m/s)	Peak ground acceleration, PGA (cm/s <sup>2</sup> )
Malatya-1	4406	37.97378 E	28	$R_1 = 143.7$	815	320	$PGA_1 = 131.34$
Malatya-2		38.34388 N	28.6	$R_2 = 70.17$		440	$PGA_2 = 467.20$
Hatay-1	3124	36.1722 E	1	$R_1 = 140.11$	283	282	$PGA_1 = 638.32$
		36.2387 N		$R_2 = 226.42$			$PGA_2 = 32.18$
Hatay-2	3136	36.24722 E	5	$R_1 = 148.38$	344	393	$PGA_1 = 534.22$
		36.11593 N		$R_2 = 236.36$			$PGA_2 = 22.79$
Gaziantep-1	2703	37.350 E	3.75	$R_1 = 37.34$	758	578	$PGA_1 = 165.06$
		37.035 N		$R_2 = 115.06$			$PGA_2 = 93.68$
Gaziantep-2	8002	36.56195 E	16	$R_1 = 43.91$	430	467	$PGA_1 = 336.56$
		37.19156 N		$R_2 = 116.24$			$PGA_2 = 65.87$
KMaraş-1	4625	36.98187 E	8.5	$R_1 = 28.40$	346	303	$PGA_1 = 466.33$
KMaraş-2		37.53872 N	6	$R_2 = 65.22$		491	$PGA_2 = 73.46$

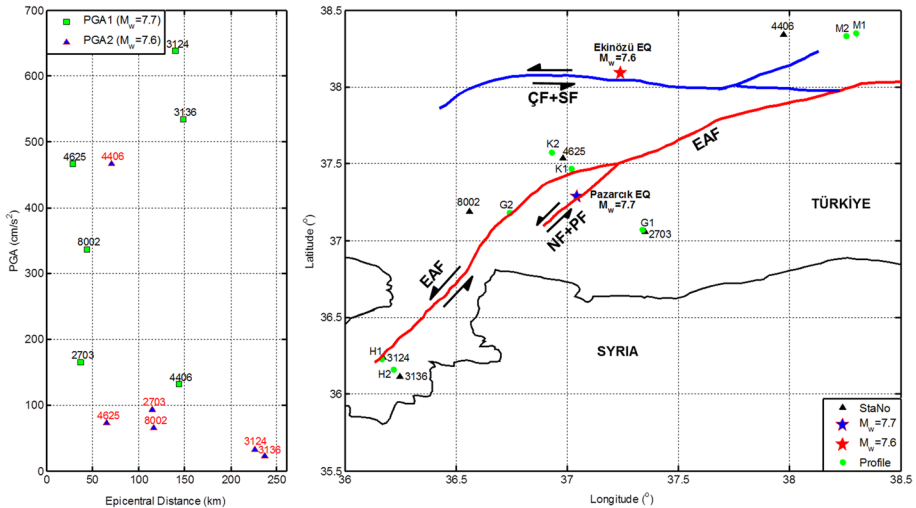


**Fig. 10** The PGA distribution and location of the stations: **a** variation of epicentral distance-PGA for nearest station locations in Table 6 and **b** locations of the station and profile according to fault directions. Faults are digitized from Melgar et al. (2023) in order to present their general directions. EAF: East Anatolian Fault, ÇF + SF: Çardak and Sürgü Faults and NF + PF: Nurdağı and Pazarçık Faults. M, G, H and K letters present profile locations in Malatya, Gaziantep, Hatay and Kahramanmaraş Provinces, respectively. The numbers of the ground motion stations closest to the survey profiles are indicated

### 5 Conclusions

The aim of this study was to investigate the soil character after two large earthquakes that occurred on February 6, 2023, and affected 11 provinces in the vicinity. For this reason, SRT, MASW and Microtremor measurements were carried out in eight different profiles in four provinces (Kahramanmaraş, Hatay, Malatya and Gaziantep) where the damage and loss of life after earthquakes were intense, and the first results obtained are presented. Also, the results obtained were correlated with the station information (epicentral distance, maximum PGA,  $V_s30$ ) closest to the measurement profiles. SRT technique provided P-wave 2D velocity-depth models, MASW technique provided 1D- $V_s$  depth profiles and MT (HVSAR) technique provided soil dominant period values. Using the velocity information, physical and geotechnical parameters of the earth materials were calculated, and soil classification was made. All but two of the measurements (Hatay-2 (Tepehan) and Kahramanmaraş-1 (Tevekkeli)) were made in settlements. However, these two points are located very close to settlements (such as villages). According to the soil classification using  $V_s30$  values, ZD (Malatya-1, Hatay-1 and Kahramanmaraş-1) and ZC (Malatya-2, Hatay-2, Gaziantep-1,2 and Kahramanmaraş-2) soil classes were determined. In all profiles, the subsurface model was determined as three-layered using SRT sections and evaluated together with the 1B- $V_s$  depth profiles, and the P- and S-wave velocities of each layer were assigned as average. In general, the high velocity ratios ( $V_p/V_s > 2.5$ ) and Poisson’s ratios ( $\sigma > 0.35$ ) explain that the near-surface geological units are very loose and the deeper rocks are very porous/fracture-cracked. The variation of dynamic-elastic parameters indicates weakly resistant geological units to depths of ~ 15–20 m in Malatya-1 (Yeşilyurt), Hatay (Defne) and

Kahramanmaraş (Tevekkeli), and moderately hard geological units to depths of ~ 10 m in Malatya-2 (Yeşilyurt), Gaziantep (İbrahimli and Nurdağı), Hatay (Defne) and Kahramanmaraş (City center). However, in all profiles, the soil units close to the surface have very low available bearing capacities (less than 4 kg/cm<sup>2</sup> or 0.4 MPa) and moderate (between 4–8 kg/cm<sup>2</sup> or 0.4–0.8 MPa) toward deeper depths. Although there is no drilling data to define the lithology, all geophysical parameters show that the deep layers (usually  $Z \geq 15$  m) in the studied locations consist of porous, weathered sedimentary rocks, while above these units, mostly very loose soil materials (clay, silt, sand, gravel and their mixture) are present. However, regardless of the soil class, according to the station information close to the measurement profile, it has been observed that stations at close epicentral distances but within the zone parallel to the direction of movement of the faults have higher acceleration values than those in perpendicular zones. These observations indicate that there is a directivity effect in the propagation of earthquake waves.

Finally, all the findings of this study reinforce the view that the damages caused by earthquake-soil structure relationship was not fully and accurately reflected in the building designs, beyond the poor quality of construction materials, subsequent interventions to the buildings and structural defects. In order to improve the results obtained in this study, both the measurement profile and the number of stations to be considered should be increased, and geophysical measurement studies should be carried out to image deeper geological structures.

**Acknowledgements** The authors would like to thank the editor and two anonymous reviewers for their constructive and developmental criticism and contributions during the revision process of the article. Earthquake data are provided by the Republic of Turkey Prime Ministry Disaster and Emergency Management Authority Presidential of Earthquake Department (AFAD; <https://deprem.afad.gov.tr/>)

**Author contributions** HK was contributed data acquisition, processing and interpretation and writing original draft. AEB was responsible for data acquisition, processing and interpretation and critically revise the manuscript. ÖA was performed data acquisition, processing and interpretation and critically revise the manuscript. All authors participated in discussions of the results and writing the manuscript. All authors read and approved the final manuscript.

**Funding** Open access funding provided by the Scientific and Technological Research Council of Türkiye (TÜBİTAK). This study was supported by project number 123D016 within the scope of Scientific and Technological Research Council of Turkey (TUBİTAK) 1002-C “Natural Disasters Focused Field Study Urgent Support Program”.

## Declarations

**Conflict of interest** The authors declare that they do not have any personal or financial conflicts of interest.

**Open Access** This article is licensed under a Creative Commons Attribution 4.0 International License, which permits use, sharing, adaptation, distribution and reproduction in any medium or format, as long as you give appropriate credit to the original author(s) and the source, provide a link to the Creative Commons licence, and indicate if changes were made. The images or other third party material in this article are included in the article's Creative Commons licence, unless indicated otherwise in a credit line to the material. If material is not included in the article's Creative Commons licence and your intended use is not permitted by statutory regulation or exceeds the permitted use, you will need to obtain permission directly from the copyright holder. To view a copy of this licence, visit <http://creativecommons.org/licenses/by/4.0/>.

## References

- AFAD (2020) Kahramanmaraş Provincial Risk Mitigation Plan on 17.08.2020 (in Turkish). Earthquake Department of Turkey's Disaster and Emergency Management Presidency, Ankara, Türkiye. <https://kahramanmaras.afad.gov.tr/il-planlari>. Accessed 05 September 2023
- AFAD (2023) 06 February 2023 Kahramanmaraş (Pazarcık and Elbistan) Earthquakes Field Works Preliminary Evaluation Report on 24 February 2023 (in Turkish). Earthquake Department of Turkey's Disaster and Emergency Management Presidency, Ankara, Turkey. [https://deprem.afad.gov.tr/assets/pdf/Arazi\\_Onrapor\\_28022023\\_surum1\\_revize.pdf](https://deprem.afad.gov.tr/assets/pdf/Arazi_Onrapor_28022023_surum1_revize.pdf), Accessed 19 September 2023
- Akın Ö, Sayıl N (2016) Site characterization using surface wave methods in the Arsin-Trabzon province NE Turkey. *Environ Earth Sci* 75:1–17
- Akkaya İ, Özvan A, Tapan M, Şengül MA (2015) Determining the site effects of 23 October 2011 earthquake (Van province, Turkey) on the rural areas using HVSR microtremor method. *J Earth Sys Sci* 124(7):1429–1443
- Ansal A, İyisan R, Güllü H (2001) Microtremor measurements for the microzonation of Dinar. *Pure Appl Geophys* 158:2525–2541
- Ansal A, Biro Y, Erken A, Gülerce Ü (2004) Seismic Microzonation: a case study. *Recent Adv Earthq Geotech Eng and Microz* 2004:253–256
- Azwin I, Saad R, Nordinac M (2013) Applying the seismic refraction tomography for site characterization. *APCBEE Procedia* 5:227–231. <https://doi.org/10.1016/j.apcbee.2013.05.039>
- Babacan AE, Gelişli K, Tweeton D (2018) Refraction and amplitude attenuation tomography for bedrock characterization: Trabzon case (Turkey). *Eng Geol* 245:344–355
- Bard PY (1998) Microtremor measurements: a tool for site effect estimation. *Effects Surface Geol Seismic Motion* 3:1251–1279
- Bauer RA, Kiefer J, Hester N (2001) Soil amplification maps for estimating earthquake ground motions in the Central US. *Eng Geol* 62:7–17
- Benson RC, Yuhr L (2002) Site characterization strategies; old and new 2nd annual conference on the application of geophysics and NDT methodologies to transportation facilities. Federal Highway Administration, Los Angeles, California
- Birgören G, Özel O, Sıyahı B (2009) Bedrock depth mapping of the coast south of Istanbul: comparison of analytical and experimental analyses. *Turk J Earth Sci* 18:315–329
- Borcherdt RD (1994) Estimates of site-dependent response spectra for design (methodology and justification). *Earthq Spectra* 10(4):617–653
- Bowles JE (1996) Foundation analysis and design, 5th edn. McGraw-Hill Book Company, New York
- Bridle R (2006) Plus/Minus refraction method applied to a 3D block. In: SEG technical program expanded abstracts. *Soci of Exp Geophys* 1421–1425.
- Buddensick ML, Sheng J, Crosby T, Schuster GT, Bruhn RL, He R (2008) Colluvial wedge imaging using traveltimes and waveform tomography along the Wasatch fault near Mapleton. *Geophys J Int* 172:686–697. <https://doi.org/10.1111/j.1365-246X.2007.03667>
- Buyuksarac A, Bekler T, Demirci A, Eysüren O (2021) New insights into the dynamic characteristics of alluvial media under the earthquake prone area: a case study for the Çanakkale city settlement (NW of Turkey). *Arab J of Geos* 14(20):1–15
- Cassaro MA, Romero EM (1987) The Mexico City earthquake-1985. ASCE, New York
- CEN (2005) Eurocode 8: design of structures for earthquake resistance- part 1: general rules, seismic actions and rules for buildings (EN 1998–1: 2004). European Committee for Normalization, Brussels
- Çetin H, Güneçli H, Mayer L (2003) Paleoseismology of the palu-lake Hazar segment of the East Anatolian Fault Zone, Turkey. *Tectonophysics* 374:163–197
- Cevher M, Keçeli AD (2018) Soil dominant period and resonance relation of building height (in Turkish). *J Appl Geophys* 17:203–224
- Duman TY, Emre Ö (2013) The East Anatolian Fault: geometry, segmentation and jog characteristics. *Geol Soc Lond Spec Publ* 372:495–529. <https://doi.org/10.1144/SP372.14>
- Emre O, Duman TY, Ozalp S, Elmaci H, Olgun S, Saroğlu F (2013) 1/1.250.000 scaled Turkey active fault map. Mineral Research and Exploration General Directorate. <http://www.mta.gov.tr/>. Accessed 10 Oct 2023
- Field EH, Jacob KH (1993) The theoretical response of sedimentary layers to ambient seismic noise. *Geophys Res Lett* 20(24):2925–2928
- Gallipoli MR, Mucciarelli M (2009) Comparison of site classification from VS30, VS10 and HVSR in Italy. *Bull Seismol Soc Am* 99:340–351

- Geldart LP, Sheriff RE (2004) Problems in exploration seismology and their solutions, SEG, Geophysical References Series No. 14, Tulsa, Oklahoma, USA
- GEOPSY, (1997). Geophysical signal database for noise array processing. <http://www.geopsy.org> Accessed June 2015.
- Goldberg DE, Taymaz T, Reitman NG, Hatem AE, Yolsal-Çevikbilen S, Barnhart WD, Irmak TS, Wald DJ, Öcalan T, Yeck WL et al (2023) Rapid characterization of the February 2023 Kahramanmaraş Turkey. *Earthq Seq Seismic Rec.* 3(2):156–167. <https://doi.org/10.1785/0320230009>
- Hodgkinson J, Brown RJ (2005) Refraction across an angular unconformity between nonparallel TI media. *Geophysics* 70:D19–D28
- Hunter JA, Woeller DJ, Addo KO, Luternauer JL, Pullan SE (1993) Application of shear wave seismic techniques to Earthquake hazard mapping in the Fraser River Delta, British Columbia. SEG Tech Program Expanded Abs 501-503
- Işık E (2023) Structural failures of adobe buildings during the February 2023 Kahramanmaraş (Turkey) earthquakes. *Appl Sci* 13:8937. <https://doi.org/10.3390/app13158937>
- Kanai K, Tanaka T (1961) On microtremors. *Bull Earthq Res Inst* 39:97–114
- Kanlı AI (2009) Initial velocity model construction of seismic tomography in near-surface applications. *J Appl Geophys* 67:52–62. <https://doi.org/10.1016/j.jappgeo.2008.09.005>
- Kaptan K, Tezcan S (2012) Examples on soil amplification of earthquake waves (in Turkish). *J Turk Sci Res Found* 5:17–32
- Karlı H, Babacan AE, Senkaya M, Gelisli K (2021) An evaluation on rippability of geological units by seismic P- and S-wave velocities (in Turkish). *Engine Sci J of Pamukkale Uni* 27(3):410–419
- Kartal RF, Kadiroğlu FT (2013) The seismotectonics of the Eastern Anatolian Fault and the statistical analysis of seismic activity along this fault over the past five years (in Turkish). 66. Türkiye Jeoloji Kurultayı, Ankara
- Keçeli AD (2012) Soil parameters which can be determined with seismic velocities. *Jeofizik* 16:17–29
- Keçeli AD, Cevher M (2015) Soil dominant period and resonance relation of building height. *Jeof Derg* 17:1–2
- Khalil MH, Hanafy SM (2016) Geotechnical parameters from seismic measurements: two field examples from Egypt and Saudi Arabia. *J Environ Eng Geophys* 21:13–28. <https://doi.org/10.2113/JEEG21.1.13>
- KOERI (2023) February 6, 2023 Mw 7.7 Gaziantep, February 6, 2023 Mw 7.6 Kahramanmaraş and February 20, 2023 Mw 6.4 Hatay Earthquakes Preliminary Evaluation Report on 13 March 2023 (in Turkish), Edited by Tanırca, G. and Eken, T.K., Kandilli Observatory and Earthquake Research Institute of Boğaziçi University (KOERI), İstanbul, Türkiye. <http://koeri.boun.edu.tr/new/sites/default/files/KRDAE-2023-Deprem-On-Degerlendirme-Raporu.pdf> Accessed 12 September 2023
- Kurtuluş C (2000) Examination of bearing capacity from seismic velocities. *Uyg Yer Bil Derg* 6:51–59
- Lachet C, Bard PY (1994) Numerical and theoretical investigations on the possibilities and limitations of Nakamura's technique. *J Phys Earth* 42(5):377–397
- Lankston RW (1989) The seismic refraction method: a viable tool for mapping shallow targets into the 1990s. *Geophys* 54:1535–1542
- Lermo J, Chavez-García FJ (1994) Are microtremors useful in site response evaluation? *Bull Seis Soc Am* 84(5):1350–1364
- Leucci G, Greco F, Giorgi LD, Mauceri R (2006) Three-dimensional image of seismic refraction tomography and electrical resistivity tomography survey in the Castle of Occhiola. *J Archaeol Sci* 34:233–242. <https://doi.org/10.1016/j.jas.2006.04.010>
- Maraio S, Bruno P, Testa G, Tedesco P, Izzo G (2014) Application of seismic refraction tomography to detect anthropogenic buried cavities in Province of Naples. *NGTTS, Trieste*
- Martínez-Pagán P, Navarro M, Pérez-Cuevas J, Alcalá FJ, García-Jerez A, Vidal F (2018) Shear-wave velocity structure from MASW and SPAC methods: the case of Adra town, SE Spain. *Near Surf Geophys* 16:356–371. <https://doi.org/10.3997/1873-0604.2018012>
- Melgar D, Taymaz T, Ganas A, Crowell BW, Öcalan T, Kahraman M, Tsironi V, Yolsal-Çevikbilen S, Valkaniotis S, Irmak TS, Eken T, Erman C, Özkan B, Doğan AH, Altuntaş C (2023) Sub- and super-shear ruptures during the 2023 Mw 7.8 and Mw 7.6 earthquake doublet in SE Türkiye, SEISMICA-FAST REPORT, Special issue for 2023 Türkiye. <https://doi.org/10.26443/seismica.v2i3.387>
- METU, 2023. Preliminary Reconnaissance Report on February 6, 2023 Kahramanmaraş-Pazarcık (Mw=7.7) and Elbistan (Mw=7.6) Earthquakes, Edited by Çetin KÖ, İlgaç M, Can G, Çakır E, Report No: METU/EERC 2023–01 Middle East Technical University (METU)/Earthquake Engineering Research Center (EERC)
- Midorikawa S (1987) Prediction of isoseismal map in Kanto plain due to hypothetical earthquake. *J Struct Dyn* 33:43–48



- Miller RD, Xia J, Park CB, Ivanov JM (1999) Multichannel analysis of surface waves to map bedrock. *The Lead Edge* 18:1392–1396
- Molina S, Navarro M, Martínez-Pagan P, Pérez-Cuevas J, Vidal F, Navarro D, Agea-Medina N (2018) Potential damage and losses in a repeat of the 1910 Adra (Southern Spain) earthquake. *Nat Hazards* 92:1547–1571. <https://doi.org/10.1007/s11069-018-3263-6>
- Molnar S, Cassidy JF, Castellaro S et al (2018) Application of microtremor horizontal-to-vertical spectral ratio (MHVSR) analysis for site characterization: state of the art. *Surv Geophys* 39(4):613–631
- Moreno DG, Hubert-Ferrari A, Moernaut J, Fraser JG, Boes X, Van Daele M, Avsar U, Çağatay N, De Batist M (2011) Structure and recent evolution of the Hazar Basin: A strike-slip basin on the East Anatolian Fault, Eastern Turkey. *Basin Res* 23:191–207
- Moustafa SS, Adel Mohamed ME, Abd El-Aal AK (2007) Applicability of near-surface seismic refraction technique to site characterization of South Marsa Matrouh and Sedi Abd El-Rahman Western Desert Egypt. *J Appl Geophys* 6(2):77–85
- Nakamura Y (1989) A method for dynamic characteristics estimation of subsurface using microtremor on the ground surface. *Railw Q* 30:25–53
- NEHRP, 2003. Recommended provisions for seismic regulations for new buildings and other structures. In: Building seismic safety council (BSSC) for the federal emergency management agency (FEMA 450). FEMA, Washington Part 1: Provisions.
- Özalaybey S, Zor E, Ergintav S, Tapırdamaz MC (2011) Investigation of 3-D basin structures in the İzmit Bay area (Turkey) by single station microtremor and gravimetric methods. *Geophys J Int* 186:883–894
- Öztürk S (2020) A study on the variations of recent seismicity in and around the Central Anatolian region of Turkey. *Phys Earth Planet Interiors* 301(106453):1–11. <https://doi.org/10.1016/j.pepi.2020.106453>
- Öztürk S, Beker Y, Sarı M, Pehlivan L (2021) Estimation of ground types in different districts of Gümüşhane province based on the ambient vibrations H/V measurements. *Sig J Eng Nat Sci* 39(4):371–394
- Ozkula G, Dowell RK, Baser T, Lin J-L, Numanoglu OA, İlhan O, Olgun CG, Huang C-W, Uludag TD (2023) Field reconnaissance and observations from the February 6, 2023, Turkey earthquake sequence. *Nat Hazards* 119:663–700
- Palutoğlu M, Şaşmaz A (2017) 29 Kasım 1795 Kahramanmaraş Depremi, Güney Türkiye (in Turkish). *Mad Tet ve Ara Derg* 155:191–206
- Pamuk E, Özdağ CÖ, Özyalın Ş, Akgün M (2017) Soil characterization of Tınaztepe region (Izmir/Turkey) using surface wave methods and Nakamura (HVSR) technique. *Earthq Eng Eng Vib* 16:447–458
- Pamuk E, Özdağ CÖ, Tunçel A, Özyalın Ş, Akgün M (2017) Local site effects evaluation for Aliğağ/İzmir using HVSR (Nakamura technique) and MASW methods. *Nat Hazards* 90:887–899. <https://doi.org/10.1007/s11069-017-3077-y>
- Park CB, Miller RD, Xia J (1999) Multichannel analysis of surface waves. *Geophys* 64(3):800–808
- Park CB, Miller RD, Xia J. (1998) Imaging dispersion curves of surface waves on multi-channel record. In: SEG technical program expanded abstracts. New Orleans, LA, pp 1377–80
- Raghu Kanth S, Iyengar RN (2007) Estimation of seismic spectral acceleration in peninsular India. *J Earth Syst Sci* 116(3):199–214
- Redpath BB (1973) Seismic refraction exploration for engineering site investigations. Technical report, E-73–4, U.S Army Engineer Waterways Experiment Station, Livermore, Calif.(USA)
- Reilinger R, McClusky, S, Vernant, P, Lawrence, S, Ergintav S, Cakmak R et al (2006) GPS constraints on continental deformation in the Africa-Arabia-Eurasia continental collisional zone and implications for the dynamics of plate interactions. *J Geophys Res Sol Earth*, 111(B5)
- Rucker ML (2000) Applying the seismic refraction technique to exploration for transportation facilities. *Geophys* 1:1–3
- Şahin Ş, Öksüm E (2021) The relation of seismic velocity and attenuation pattern in the East Anatolian fault zone with earthquake occurrence: Example of January 24, 2020 Sivrice Earthquake. *Bull Min Res Exp* 165:141–161
- Salem HS (2000) The compressional to shear-wave velocity ratio for surface soils and shallow sediments. *Eur J Environ Eng Geophys* 5:3–14
- SeisImager/SW (2022). Manual V 1.4 WindowsTM Software for Analysis of Surface Waves (V. 7.6), Including explanation of geometrics seismodule controller software surface wave data acquisition wizards. <ftp://geom.geometrics.com/pub/seismic/SeisImager>. Accessed July 2023
- SESAME (2004) Guidelines for the implementation of the H/V spectral ratio technique on ambient vibrations: measurements, processing and interpretations, SESAME European Research Project WP12— D23.12. [www.geopsy.org](http://www.geopsy.org) Accessed June 2020.
- Sheehan RJ, Doll EW, Wayne AM (2005) An evaluation of methods and available software for seismic refraction tomography analysis. *J Environ Eng Geophys* 10:21–34

- Sitharam TG, James N, Kolathayar S (2018) Comprehensive seismic zonation schemes for regions at different scales. Springer, Berlin
- Tatham RH (1982) Vp/Vs and lithology. *Geophys* 47:336–344
- TEBC (Turkey Earthquake Building Code) (2018) Türkiye earthquake and building regulations (in Turkish), Ministry of Environmental, Climatic and Urbanisation, Turkey
- Telford W, Geldart L, Sheriff R, Keys D (1976) Applied geophysics. Cambridge University Press, New York
- Tezcan SS, İpek M (1973) Long distance effects of the March 28, 1970 Gediz Turkey. *Earthq Earth Eng Struct Dyn* 1:203–215
- Tezcan SS, Yerlici V, Durgunoğlu HT (1978) A Reconnaissance for the Romanian earthquake of March 4, 1977. *Earth Eng and Str Dyn* 6:379–421
- Tezcan SS, Özdemir Z, Keçeli AD (2009) Seismic technique to determine the allowable bearing pressure for shallow foundations in soils and rocks. *Act Geophys* 57(2):400–412. <https://doi.org/10.2478/s11600-008-0077-z>
- Tinsley JC, Fumal TE (1985) Mapping Quaternary sedimentary deposits for areal variations in shaking response. *Evaluating Earthq Hazards Los Angeles Reg-An Earth SciPerspect* 1360:101–126
- Tun M, Pekkan E, Ozel O, Guney Y (2016) An investigation into the bedrock depth in the Eskisehir Quaternary Basin (Turkey) using the microtremor method. *Geophys J Int* 207(1):589–607
- Uhlemann S, Hagedorn S, Dashwood B, Maurer H, Gunn D, Dijkstra D, Chambers J (2016) Landslide characterization using P and S-wave seismic refraction tomography—the importance of elastic moduli. *J Appl Geophys* 134:64–76
- Uyanık O (2011) The porosity of saturated shallow sediments from seismic compressional and shear wave velocities. *J Appl Geophys* 73(1):16–24
- Uyanık O (2019) Estimation of the porosity of clay soils using seismic P- and S-wave velocities. *J Appl Geophys* 170:103832
- Uyanık O, Çatlıoğlu B (2015) Determination of density from seismic velocities (in Turkish). *Jeofizik* 17:3–15
- Uyanık O, Gördesli F (2013) Examination of bearing capacity from seismic velocities (in Turkish). *SDU Int Technol Sci* 5(2):78–86
- Vanlı Senkaya G, Senkaya M, Karşlı H, Güney R (2020) Integrated shallow seismic imaging of a settlement located in a historical landslide area. *Bull Eng Geol Environ* 79:1781–1796. <https://doi.org/10.1007/s10064-019-01612-0>
- Xia J, Miller RD, Park CB (1999) Estimation of near-surface shear-wave velocity by inversion of Rayleigh wave. *Geophys* 64(3):691–700
- Xia, J, Miller RD, Park CB (1998) Construction of vertical section of near-surface shear wave velocity from ground roll: technical program. In: The society of exploration geophysicists and the Chinese petroleum society Beijing 98, International Conference 29:33
- Yılmaz O, Eser M, Berilgen M (2009) Applications of engineering seismology for site characterization. *J Earth Sci* 20(3):546–554
- Yılmaz O, Eser M, Berilgen M (2006) Seismic, geotechnical, and earthquake engineering site characterization. SEG Technical Program Expanded Abstracts Soc Explor Geophys pp 1401–1405
- Zhu X, McMechan GA (1989) Estimation of two-dimensional seismic compressional wave velocity distribution by interactive tomographic imaging. *Int J Im Sys Tech* 1(1):13–17
- Zor E, Özalaybey S, Karaaslan A, Tapırdamaz MC, Özalaybey ÇS, Tarancıoğlu A, Erkan B (2010) Shear wave velocity structure of the İzmit Bay area (Turkey) estimated from active–passive array surface wave and single-station microtremor methods. *Geophys J Int* 182(3):1603–1618

**Publisher's Note** Springer Nature remains neutral with regard to jurisdictional claims in published maps and institutional affiliations.